MJO and Tropical Cyclogenesis in the Gulf of Mexico and Eastern Pacific: Case Study and Idealized Numerical Modeling

ANANTHA AIYYER

Department of Marine, Earth, and Atmospheric Sciences, North Carolina State University, Raleigh, North Carolina

JOHN MOLINARI

Department of Earth and Atmospheric Sciences, University at Albany, State University of New York, Albany, New York

(Manuscript received 15 November 2006, in final form 4 June 2007)

ABSTRACT

The role of the Madden–Julian oscillation (MJO) in modulating the frequency and location of tropical cyclogenesis over the eastern Pacific and the Gulf of Mexico during August–September 1998 is examined. During the nonconvective phase of the MJO, convection and low-level cyclonic vorticity occurred primarily in conjunction with the intertropical convergence zone (ITCZ). During the convective phase, convection, low-level cyclonic vorticity, and convergence expanded into the northeastern Pacific and the Gulf of Mexico. This was accompanied by enhanced eddy kinetic energy and barotropic energy conversions as compared to the nonconvective phase, consistent with previous research. During the nonconvective phase of the MJO, vertical shear was relatively weaker but tropical cyclones tended to form mainly within the ITCZ. On the contrary, during the convective phase, vertical wind shear exceeded 10 m s^{-1} over much of this region and tropical cyclone development occurred north of the ITCZ, near the Mexican Pacific coast and the Gulf of Mexico.

Idealized numerical experiments are conducted using a barotropic model with time-invariant basic states representative of the nonconvective and convective phases of the MJO. The simulations indicate that the propagation paths as well as the amplification of the eddies differ substantially between the two phases. During the nonconvective phase, the waves tend to propagate westward into the eastern Pacific. During the convective phase, stronger southerlies steer the waves into the Gulf of Mexico. The MJO-related modulation of tropical cyclogenesis in the eastern Pacific and Gulf of Mexico thus appears to involve anomalous convergence, cyclonic vorticity, vertical wind shear, and differing tracks of easterly waves.

1. Introduction

Tropical cyclogenesis is a complex process that spans multiple spatial and temporal scales. The large-scale environment plays a central role in this process. The accumulated evidence from past studies has firmly established the importance of the dynamic state (e.g., low-level relative vorticity, vertical wind shear) and the thermodynamic state (e.g., sea surface temperature, air–sea thermal disequilibrium) of the environment in influencing the genesis and development of tropical cyclones (e.g., Palmen 1948; Gray 1968; Emanuel 1986). An increasing emphasis in the literature is being placed on sources of intraseasonal variability such as the Madden–Julian oscillation (MJO; Madden and Julian 1971), spurred by the recognition that the associated changes in the environment can modulate tropical cyclone (TC) activity. Nakazawa (1986) analyzed the distribution of global TCs during 1979 and found that they tended to form within the convective envelope of the MJO. This result was confirmed in subsequent studies that used longer data record for the Indian and western Pacific (Liebmann et al. 1994; Hall et al. 2001), eastern North Pacific (Maloney and Hartmann 2000a), and the Gulf of Mexico (Maloney and Hartmann 2000b).

Previous studies (e.g., Liebmann et al. 1994) have found that the environment associated with the convective phase of the MJO consists of anomalous low-level cyclonic vorticity and convergence, two key ingredients that favor cyclogenesis (e.g., Gray 1968; McBride and Zehr 1981). Maloney and Hartmann (2000a, 2001) used

Corresponding author address: Anantha Aiyyer, Department of Marine, Earth, and Atmospheric Sciences, Campus Box 8208, North Carolina State University, Raleigh, NC 27695-8208.
E-mail: aaiyyer@ncsu.edu

DOI: 10.1175/2007JAS2348.1

the leading empirical orthogonal function of the 850-hPa zonal wind to define the phase of the MJO over the eastern Pacific. Their composite at 850 hPa for the convective phase consists of an anomalous westerly jet at around 10°N in the eastern Pacific and cyclonic gyres to the north over the eastern Pacific and the Gulf of Mexico. The MJO wind anomalies at the lower and upper levels also impact the environmental vertical shear. Maloney and Hartmann (2000a) argued that the vertical shear during the convective phase of the MJO is more conducive for cyclogenesis than the nonconvective phase. They also reported that, over the eastern Pacific, TCs are 4 times more likely to form during the MJO's convective phase than during its nonconvective phase.

Past studies have also shown that, to the first order, barotropic dynamics can be invoked to understand the impact of the MJO on the growth of TC precursors. Molinari et al. (1997) suggested that the MJO-related reversal in low-level potential vorticity gradient provides a mechanism for amplification of waves arriving from upstream. Sobel and Maloney (2000) showed that barotropic wave activity flux convergence is enhanced during the convective phase of the MJO, indicating that wave accumulation (Holland 1995) plays a potentially important role in the amplification of incident waves. Maloney and Hartmann (2001) and Hartmann and Maloney (2001) found significant barotropic energy conversions from the mean state to the eddies during the convective phase of the MJO, and suggested that this is a useful framework for interpreting the modulation of tropical cyclogenesis by the MJO.

To further clarify the relationship between the MJO and tropical cyclogenesis, climatology-based statistics from past investigations need to be augmented with detailed case studies. While the eastern Pacific has received focused attention (Molinari et al. 1997; Molinari and Vollaro 2000), a case study of the MJO-related tropical cyclogenesis within the Gulf of Mexico has not been reported in the literature. This paper focuses on one such case of MJO-related tropical cyclogenesis in the Gulf of Mexico and eastern Pacific. The goals of this study are to examine 1) the evolution of the environmental flow associated with the MJO and 2) the evolution of easterly waves within the MJO background flow.

In this paper, the events leading to the formation of five TCs between 31 August and 17 September (Fig. 1) are studied, and it is suggested that the clustering of these storms was related to the passage of the MJO. The results show that easterly waves arriving from upstream amplified within the environment associated with the convective phase of the MJO. These amplifying waves are hypothesized to have served as precursor disturbances to TCs. The convective MJO phase is compared with the preceding nonconvective phase during which three TCs occurred. Vertical shear and barotropic energetics for the two periods are examined. Consistent with past climatological studies, it is found that the barotropic growth rates are higher during the convective phase of the MJO. However, it is found that the vertical shear is also higher during the convective phase. This implies that the convective phase of the MJO is not uniformly conducive to TC formation and that genesis tends to occur under competing influences of favorable background convergence and vorticity and unfavorable vertical wind shear. It is suggested that this may in part have contributed to the northward shift in the genesis location of TCs during the convective phase of the MJO.

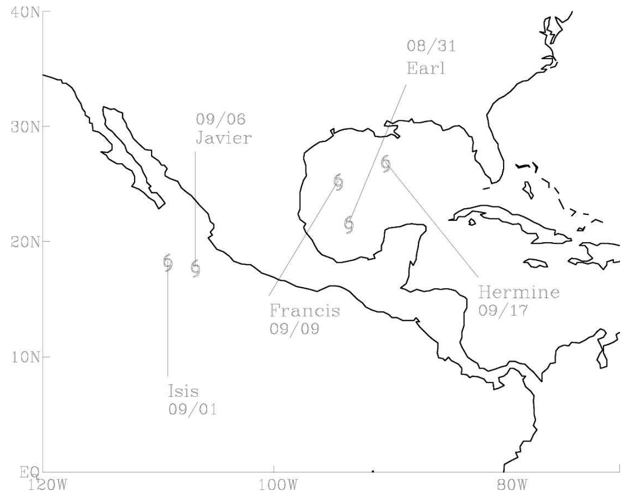

FIG. 1. The hurricane symbols represent initial locations of TCs from the National Hurricane Center (NHC) best track dataset regardless of the lat.

2. Data and method

This study uses uninitialized gridded analyses from the European Centre for Medium-Range Weather Forecasts (ECMWF). The ECMWF data are on 1.125° latitude–longitude grids. The utility of the ECMWF analyses and their limitations have been extensively discussed in Molinari and Vollaro (1990) and Molinari et al. (1992). We also use global brightness temperatures (T_b) from the Cloud Archive User Service (CLAUS) as a proxy for deep tropical convection. Details about the CLAUS dataset are provided in Hodges et al. (2000).

The definition of the seasonal mean will refer to the average over the months July–October. We use 20-day low-pass and 2–6-day bandpass time-filtered fields to describe, respectively, the slowly varying environment and wave-scale eddy fields. The time filtering is performed using the Lanczos filter (Duchon 1979). As noted in Molinari and Vollaro (2000), the 20-day low-pass filter provides a reasonable depiction of the MJO and the anomalies of this data relative to the seasonal mean are effectively equivalent to 20–90-day band-passed fields that are commonly used to study the MJO. To present further evidence of the MJO during August–September 1998, we also perform a wavenumber-frequency spectrum analysis as described in Wheeler and Kiladis (1999). The MJO signal in the CLAUS T_b is extracted by retaining only those spectral components that correspond to wavenumbers 0–9 and periods 30–96 days.

This study covers the period 9 August–17 September 1998, which encompasses a strong convective MJO phase and its preceding nonconvective phase over the Gulf of Mexico and eastern Pacific.

3. Large-scale evolution

Figure 2 shows the longitude–time diagram of the unfiltered T_b (in color shading), averaged over the latitudes 10°–20°N, for the entire season. Also shown are TCs at their genesis longitude when first named, regardless of their latitude. A series of westward-moving disturbances can be seen throughout the season. It is readily apparent that most of the TCs in Fig. 2 originate from these easterly waves that can be tracked across the Caribbean.

In addition to the westward-moving disturbances, Fig. 2 also contains large-scale eastward-propagating convective clusters. A prominent cluster is evident during 29 August–17 September. These eastward-propagating features are clearly identified by the black contours that depict the T_b filtered for the MJO band following Wheeler and Kiladis (1999). While not every TC shown in Fig. 2 forms in association with an MJO event, two prominent clusters of storms do. One of them occurs during late August and early September, and the other during mid-October. Focusing on the former, it is seen that the convective activity can be tracked from the central Pacific and amplifies when it reaches the eastern Pacific. As noted earlier in Fig. 1, five TCs originated within the convective envelope of this MJO event,

Figure 3 shows the latitude–time diagram of the MJO band T_b, averaged over the longitudes 100°–90°W. The on–off periods of MJO convection are again clearly seen in this figure. The northward shift of convection associated with MJO during 29 August–17 September is evident from the downward slope of the axis of maximum T_b. Figure 3 also shows that, on average, the latitude of formation of TCs is higher during the convective phase of the MJO than during the nonconvective phase. During the nonconvective phase, tropical cyclogenesis appears more likely to occur within the intertropical convergence zone (ITCZ).

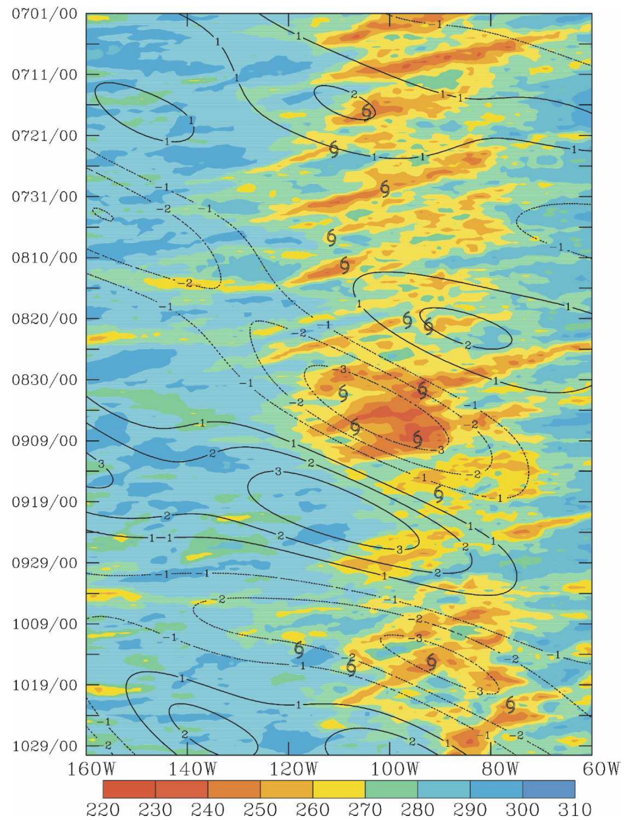

FIG. 2. Lon–time diagram of unfiltered (shaded) and MJO-band (contours) brightness temperature (K) averaged over the latitudes 5°–20°N during July–October 1998. The hurricane symbols represent initial locations of TCs from the NHC best track dataset regardless of the lat.

The picture that emerges from Figs. 2 and 3 is consistent with the findings of Molinari and Vollaro (2000), who showed cases of eastern Pacific TCs that were initiated by amplifying easterly waves within the envelope of eastward-propagating MJO superclusters. In the remainder of this section, we examine the large-scale evolution, focusing on the period highlighted above. We will provide further evidence to support the suggestion that the large scale was characterized by the MJO as seen in the convective and dynamical fields.

a. MJO evolution

Figure 4 shows a sequence of low-pass-filtered T_b and 850-hPa winds and provides a description of the evolu-

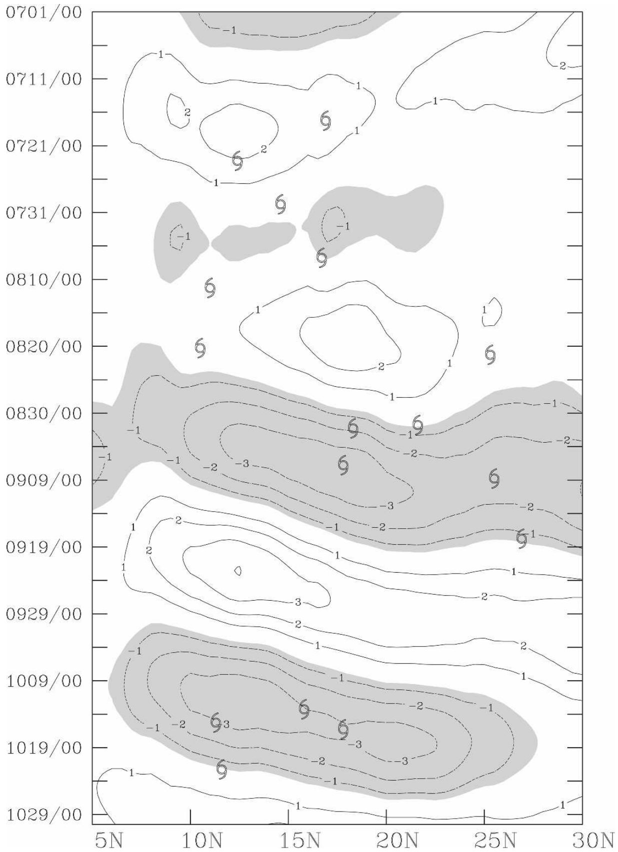

FIG. 3. Lat–time diagram of brightness temperature (K; negative values shaded) filtered for the MJO band, averaged over the lon 120°–75°W. The hurricane symbols represent initial locations of TCs within the eastern Pacific and the Gulf of Mexico.

tion of the large-scale environment over a period of 35 days. The first panel (0000 UTC 15 August; Fig. 4a) shows a nearly zonal area of convection centered on 10°N, and reflects the position of the ITCZ over the eastern Pacific. Convective activity can also be seen over the land area of the Americas but it is relatively inactive within the Gulf of Mexico. A broad area of easterlies exists between 10° and 20°N across the entire eastern Pacific and the Caribbean. Equatorward of the ITCZ axis, the southeasterly trades are also clearly seen. The circulation within the Gulf of Mexico appears to be weakly anticyclonic at this time.

A week later (Fig. 4b), there is a hint of the appearance of westerly flow between 130° and 110°W at the latitude of the ITCZ and a weak cyclonic circulation just poleward of it. This picture becomes much clearer in the next panel (0000 UTC 29 August; Fig. 4c), which shows that westerly flow has supplanted the easterlies within the eastern Pacific. Convection has spread poleward over northeastern Pacific and southwestern Gulf of Mexico. Two cyclonic gyres can also be seen—one over the eastern Pacific and the other, which is relatively weaker, over the Gulf of Mexico. By 5 September (Fig. 4d), deep convection has progressed further northward in the eastern Pacific and now covers the entire Gulf of Mexico. Both cyclonic gyres have strengthened and moved northward. The deepest convection in the eastern Pacific is now clearly north of the initial ITCZ axis.

The next panel (0000 UTC 12 September; Fig. 4e) shows that the convection over the eastern Pacific has diminished while it is still active over the Gulf of Mexico. By 19 September (Fig. 4f), the convective activity is mostly confined within the Gulf of Mexico while a weak ITCZ can be seen in the eastern Pacific. The ITCZ appears to be narrow and fractured. The initial structure of the ITCZ seen in Fig. 4a is reestablished after about 7 days (not shown).

The sequence of events seen in Fig. 4 is consistent with the development of the MJO within the eastern Pacific during 1991 as described by Molinari and Vollaro (2000). However, unlike in 1991, in the present case the MJO progresses further eastward and northward within the Gulf of Mexico. The structure of the wind field in Fig. 4 is similar to the composite MJO during its convective phase as shown by Maloney and Hartmann (2000b; their Fig. 1a).

Since the evidence for the MJO has been presented by employing filtering techniques, the possible projection of the TC signal on the filtered fields must be addressed. An examination of the unfiltered data during days with no TCs between 29 August and 17 September reveals convective activity and low-level cyclonic circulations over the Gulf of Mexico and eastern Pacific (not shown), consistent with the filtered MJO fields. Furthermore, in their summaries of the 1998 hurricane activity, Pasch et al. (2001) and Avila and Guiney (2000) also noted persistent low-level cyclonic circulations in the two basins during this period. However, it is still possible that TCs project somewhat onto the circulation attributed to the MJO merely because of the artifact of filtering. Nonetheless, as in any study incorporating spectral filtering, it is anticipated that this effect does not significantly alter the gross structure of the MJO.

b. *Composites for nonconvective and convective MJO phases*

In the following sections, the period 29 August–17 September will be referred to as the convective phase of MJO and will be contrasted with the preceding 20 days from 9 August to 28 August. The latter will be referred to as the nonconvective phase of the MJO.

Figure 5 shows the composite unfiltered 850-hPa di-

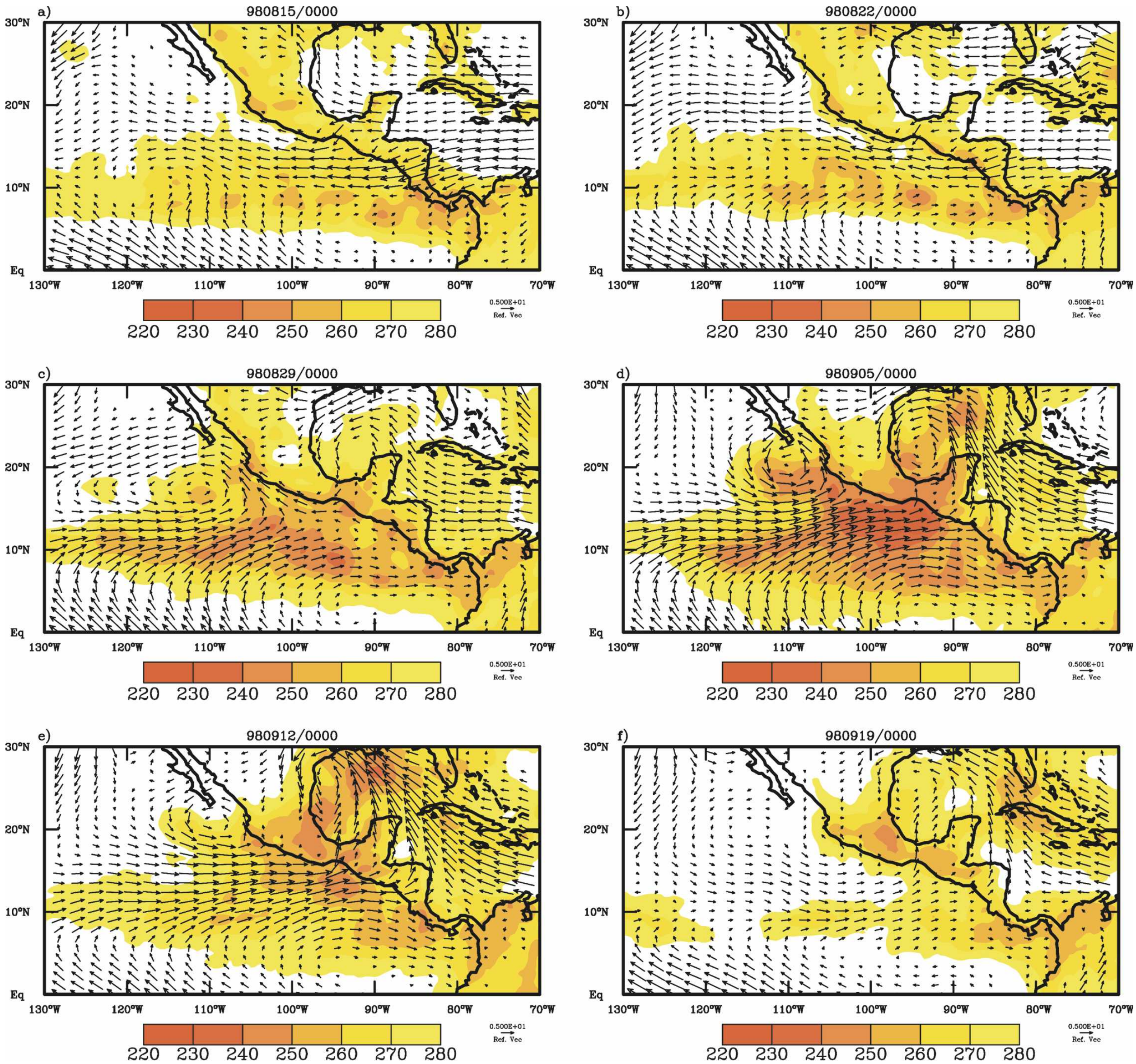

FIG. 4. Snapshots of 20-day low-pass-filtered brightness temperature (K; shaded) and 850-hPa winds (m s^{-2}; vectors) shown one week apart, starting at 0000 UTC 15 Aug 1998.

vergence and vorticity for the aforementioned periods. During the nonconvective phase, a nearly zonally oriented strip of convergence exists along 10°N over the eastern Pacific (Fig. 5a). The relative vorticity field for the same period has smaller-scale local extrema over the topographical features of Central America, but a strip of positive vorticity can be seen extending from the Caribbean to the eastern Pacific (Fig. 5b). The convergence and the vorticity fields in Figs. 5a,b are consistent with the definition of the ITCZ over the eastern Pacific (e.g., Molinari and Vollaro 2000). During this period, the Gulf of Mexico is not associated with any appreciable low-level convergence and cyclonic relative vorticity in these composite fields.

The composite divergence field for the convective phase of the MJO includes the signals of both the ITCZ and the MJO (Fig. 5c). The ITCZ can be seen as the elongated region of convergence, again centered on 10°N. However, east of 105°W, the convergence extends northward of the mean ITCZ position. In this composite, the convergence maximum is found not in the ITCZ, but within the Gulf of Mexico and clearly reflects the MJO's incursion into this region. In association with the convergence in the Gulf of Mexico and

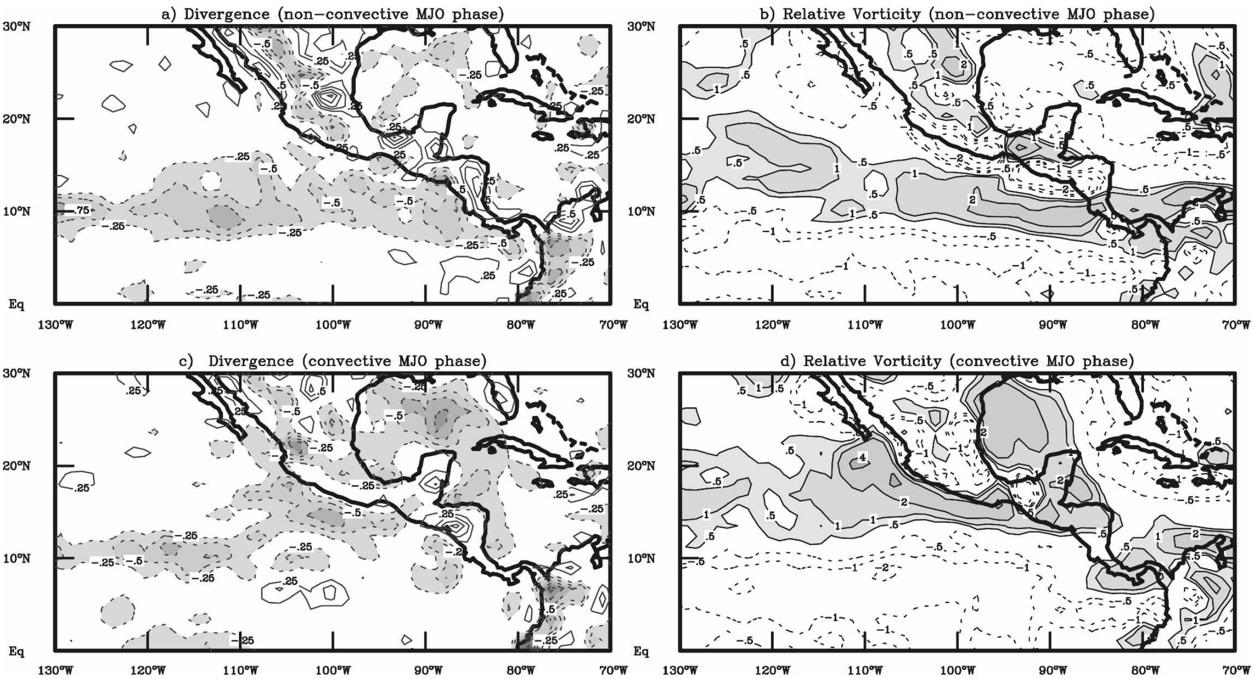

FIG. 5. Composite unfiltered 850-hPa divergence (10^{-5} s^{-1}; negative values shaded) during (a) nonconvective phase and (c) convective phase of the MJO. Composite unfiltered 850-hPa vorticity (10^{-5} s^{-1}; positive values shaded) during (b) nonconvective and (d) convective phase of the MJO.

northeastern Pacific, two distinct cyclonic gyres are also evident (Fig. 5d). The presence of low-level convergence and positive relative vorticity within the Gulf of Mexico and northeastern Pacific during the MJO's convective phase indicates an environment that is conducive to tropical cyclogenesis (e.g., McBride and Zehr 1981).

Since the MJO contains wind anomalies at both lower and upper levels, it also modulates the environmental vertical shear. Figure 6 shows the composite of the 200–850-hPa vertical shear during the two phases of the MJO. Both zonal and meridional winds at the two levels are used to compute the vertical shear. During the nonconvective phase (Fig. 6a), the mean vertical shear is large south of the ITCZ axis, but is relatively weak over the Gulf of Mexico and the northeastern Pacific. The three TCs during this period formed within relatively low ambient shear conditions. Both eastern Pacific storms formed in the vicinity of the ITCZ, consistent with the climatologically favored locations of tropical cyclogenesis in this basin.

The composite for the MJO's convective phase (Fig. 6b) shows a significant difference in the shear pattern as compared to the nonconvective period. The convective phase is associated with strong westerly low-level winds (Figs. 4c–e) and easterly upper-level winds (not shown), and leads to high shear values in the eastern Pacific. This is reflected in the secondary shear maximum north of the ITCZ axis in Fig. 6b. The strong low-level cyclonic gyre (Fig. 5d) and the associated upper-level anticyclonic outflow (not shown) also combine to produce high shear values over the Gulf of Mexico. The two storms that form within the eastern Pacific occurred around 18°N, which is north of the climatologically favored genesis latitude in this basin. The presence of large shear values between 10°–15°N is the likely cause for the northward shift in the formation of these two storms. Of the three storms in the Gulf of Mexico, two formed in a relatively low shear environment over the western part of the Gulf. The ambient mean shear around the location of the third tropical storm was around 16 m s^{-1}, a value larger than the commonly recognized threshold of 10–12 m s^{-1} (e.g., Zehr 1992) for favorable shear.

The results in this section indicate that the environment associated with the convective phase of the MJO has complex characteristics. While the low-level convergence and vorticity in the Gulf of Mexico and the northeastern Pacific are favorable, the vertical shear is not uniformly conducive to tropical cyclogenesis. In this case, the vertical shear is high over a significant portion of the Gulf of Mexico and the eastern Pacific. Despite the enhanced shear, five TCs formed within this region, and this suggests the importance of the favorable influ-

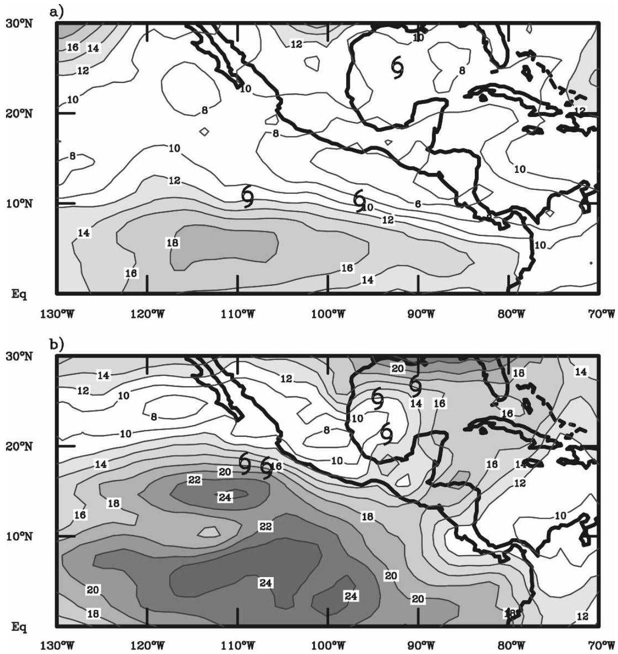

FIG. 6. Composite unfiltered 200–850-hPa vertical shear (m s^{-1}; >12 shaded) for (a) the nonconvective phase of MJO (9–28 Aug 1998) and (b) the convective phase of MJO (29 Aug–17 Sep 1998). Hurricane symbols depict the initial locations of TCs during the respective periods.

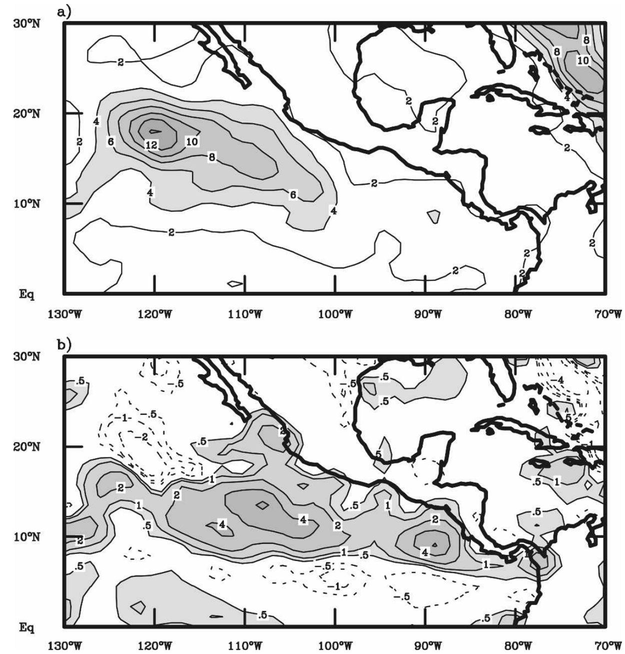

FIG. 7. (a) Mean 850-hPa EKE (m^2 s^{-2}; values >4 shaded) and (b) mean 850-hPa EKE rate of change (m^2 s^{-2} day^{-1}; values >0.5 shaded) through barotropic energy conversions from the basic state during the nonconvective phase of MJO (9–28 Aug 1998).

ence of the low-level convergence and relative vorticity associated with the convective phase of the MJO.

c. Barotropic energetics

The previous sections have highlighted the differences in the environmental conditions during the convectively active and inactive MJO periods. Corresponding differences in the number and genesis locations of TCs were also noted and were related qualitatively to the large-scale dynamical fields for the respective periods. Following Maloney and Hartmann (2001), a quantitative assessment of the differing impact of the two phases of the MJO can be made by examining the growth of the precursor disturbances via barotropic processes.

For a barotropic fluid, linearized about a time-invariant basic state, the exchange of kinetic energy between the eddies and the basic state (environment) is encapsulated in the following expression:

$$C(\overline{K}, K')_{\text{baro}} = -u'u'\frac{\partial \overline{u}}{\partial x} - u'v'\frac{\partial \overline{u}}{\partial y} - u'v'\frac{\partial \overline{v}}{\partial x} - v'v'\frac{\partial \overline{v}}{\partial y}, \tag{1}$$

where $C(\overline{K}, K')_{\text{baro}}$ denotes the eddy kinetic energy (EKE) growth rate, u and v are, respectively, the zonal and meridional components of velocity, and $K = ½(u^2 + v^2)$ is the kinetic energy. The terms with overbars represent the basic state and those with primes denote the eddies. The four terms on the rhs of (1) are commonly referred to as the barotropic conversion terms (e.g., Wiin-Nielsen 1961; Maloney and Hartmann 2001). For the results described in this section, the 20-day low-pass-filtered fields are used to compute the basic states. The eddies are defined using 2–6-day bandpass-filtered fields. The choice of this band to define the eddies is consistent with range of periods associated with easterly waves (e.g., Carlson 1969).

Figure 7a shows the 850-hPa EKE averaged over the nonconvective phase of the MJO. The most significant area of mean eddy activity lies over the eastern Pacific, westward of 100°W. The mean EKE in this region reaches a peak of 14 m^2 s^{-2} around 120°W and 18°N. Significant EKE values can also be seen in the Atlantic, east of 80°W. However, these local maxima in EKE may in part reflect the tracks of TCs themselves. During this period, the Gulf of Mexico exhibits very weak eddy activity with mean EKE values only in the range of 2–3 m^2 s^{-2}. Figure 7b shows the average 850-hPa EKE growth rate as a result of barotropic energy conversions from the basic state. The most prominent area of eddy growth is the zonally elongated region in the vicinity of the ITCZ in the eastern Pacific. The highest value here

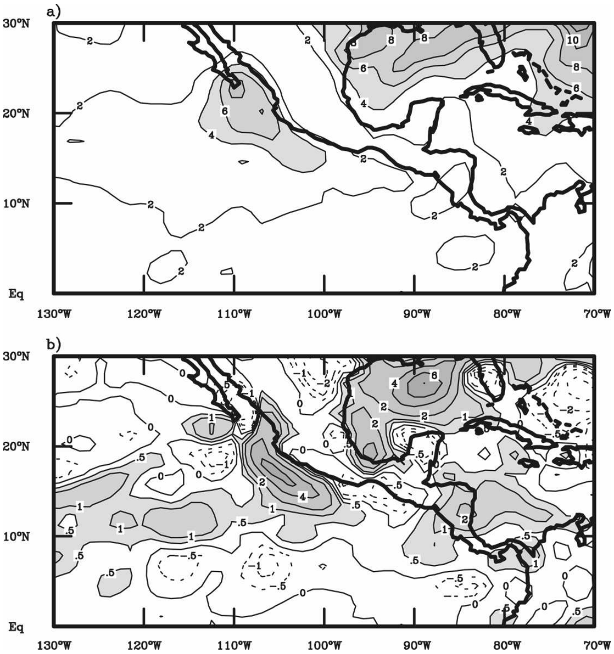

FIG. 8. As in Fig. 7, but for the convective phase of MJO (29 Aug–17 Sep 1998).

is 6 $m^2 s^{-2} day^{-1}$. However, within the Gulf of Mexico, the barotropic conversions are only within 0.5–1.0 $m^2 s^{-2} day^{-1}$, indicating negligible eddy growth during the nonconvective MJO phase. This is consistent with the weak EKE values seen in Fig. 7a.

Figure 8a shows the EKE averaged over the convective phase of the MJO. A comparison with Fig. 7 reveals a clear shift in the location of the peak eddy activity. During this period, the highest EKE occurs in the Gulf of Mexico. The EKE in this region exceeds 3 $m^2 s^{-2}$, with peak values around 10 $m^2 s^{-2}$. In the eastern Pacific, the mean EKE pattern is less expansive and has shifted northeastward as compared to the nonconvective MJO phase. The peak EKE values now exist just west of the coast of Mexico and exceed 8 $m^2 s^{-2}$. The mean EKE growth rate due to the barotropic conversions (Fig. 8b) also reflects this northward shift in eddy activity. The most striking change from the nonconvective MJO phase is the presence of positive barotropic conversions over most of the Gulf of Mexico, indicating net eddy growth during this period. The growth rate reaches 8 $m^2 s^{-2} day^{-1}$, and a comparison with Fig. 8a suggests that this rate of energy conversion is sufficient to achieve the mean EKE level on time scales of 2–3 days. High rates of eddy growth can also be seen along the west coast of Mexico, between 15°–20°N, and this is reflected in the mean EKE pattern in Fig. 8a. This is consistent with the observations of Molinari and Vollaro (2000), who showed that synoptic-scale easterly waves regularly reach the Caribbean and the eastern Pacific and amplify within the convective envelope of the MJO. The present case study indicates that a similar behavior occurs within the Gulf of Mexico.

The results in this section have provided a measure of the differing impact of the mean flow on eddy growth during the nonconvective and convective phases. In the former, the eddy growth occurs within the ITCZ, while in the latter the eddy growth shifts northeastward into the Gulf of Mexico. Thus, even though the details of the development of the eddies, and their transformation into TCs, must undoubtedly depend on dynamical and thermodynamical processes not considered here, a simple barotropic framework provides some insight into the impact of the MJO on the growth of the precursor disturbances.

From Figs. 7 and 8, it can be noted that the genesis locations of TCs also coincides with the regions of peak eddy growth. While this suggests that the barotropic calculations have correctly identified the regions of eddy growth, there again exists the possibility that the eddy growth may, in fact, represent the projection of the TCs onto the filtered data, in particular the 2–6-day bandpassed eddy fields. In the following section, we use an idealized barotropic model to show that growing waves within the convective MJO basic state also lead to a similar pattern of eddy activity even in the absence of a direct effect of TCs.

4. Idealized barotropic modeling

In the previous section, it was suggested that the mean flow associated with the convective phase of the MJO fosters the growth of eddies within the Gulf of Mexico. It was also suggested that the eddies represent easterly waves that arrive from upstream. The results in this section show that a barotropic model with a Rossby wave source, when linearized about a time-invariant mean flow representative of the convective phase of the MJO, simulates the growth of eddies similar to that seen in observations.

The linearized barotropic vorticity equation on the sphere with a Rossby wave generator, Rayleigh friction, and biharmonic diffusion can be written as

$$\frac{\partial \zeta'}{\partial t} + \left(\frac{\overline{u}}{r}\frac{1}{\cos\theta}\frac{d\zeta'}{d\lambda} + \frac{\overline{v}}{r}\frac{d\zeta'}{d\theta}\right) + J(\psi', \overline{\zeta} + f) + \overline{D}\zeta' = F(\lambda, \theta, t) + \alpha\nabla^4\zeta + \epsilon\zeta, \quad (2)$$

with

$$J(A, B) = \frac{1}{r^2\cos\theta}\left(\frac{dA}{d\lambda}\frac{dB}{d\theta} - \frac{dB}{d\lambda}\frac{dA}{d\theta}\right), \quad (3)$$

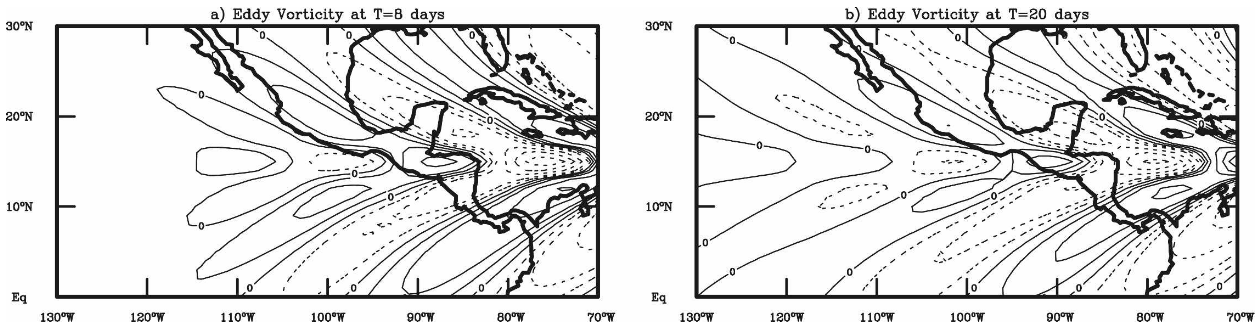

FIG. 9. Eddy vorticity after (a) 8 days and (b) 20 days of integration of the barotropic model with a Rossby wave forcing centered at 30°W, 15°N. Basic state consists of a uniform easterly flow. Geography is shown only for reference.

where the prime terms denote the eddies and the bar terms denote the basic state, and θ and λ are, respectively, the latitude and longitude. The rest of the variables are streamfunction (ψ), Coriolis parameter (f), vorticity (ζ), and the wind components (u, v).

The equation is cast into finite difference form and integrated in time using the third-order Adams–Bashforth scheme. The model's zonal extent equals the earth's circumference and the meridional extent is confined to a channel between 20°S and 40°N. A uniform grid spacing of 1° and a time step of 300 s are used. The coefficient for the biharmonic diffusion (α) is chosen such that the smallest resolved waves are damped with an e-folding time scale of 3 days, and the time scale for the Rayleigh friction ($1/\epsilon$) is 5 days. The structure of the Rossby wave forcing (F) is adapted from Kuo et al. (2001):

$$F = A\cos\left(2\pi\frac{\theta-\theta_o}{\theta_r}\right)\exp\left(-\frac{\lambda-\lambda_o}{\lambda_r}\right)\sin\left(\frac{2\pi t}{T}\right),$$
$$-\theta_r/4 \le \theta \le \theta_r/4. \tag{4}$$

The Rossby wave forcing is centered at $\lambda_o = 30°W$, $\theta_o = 15°N$, with meridional scale $\theta_r = 7°$, and zonal e-folding scale $\lambda_r = 1°$. The period of oscillation (T) is set to 3.5 days and the amplitude $A = 8 \times 10^{-13}\ \mathrm{s}^{-2}$. The eddy vorticity is inverted at each time step using the algorithm described in Sweet (1977).

Each simulation is carried out for an initial adjustment period of 5 days, followed by an integration for 20 days. All results in this section pertain to the postadjustment, 20-day integration period. The results are qualitatively similar for reasonable changes in the forcing parameters. Since in the linear model the eddies can be scaled arbitrarily as long as the linearity conditions are satisfied, all fields pertaining to the eddies will be reported in nondimensional units. Thus, a direct comparison of the magnitudes of the observed and simulated barotropic energetics will not be made. Instead, the spatial structure of the mean EKE and barotropic conversions is of greatest interest. However, since the model parameters do not vary between simulations, the structure as well as the magnitude of the eddies in nonconvective and convective MJO simulations can be directly compared.

The first simulation uses a uniform basic state to examine the eddy structures in a background without zonal and meridional inhomogeneities. Figure 9 shows the eddy vorticity induced by the Rossby wave forcing when the basic state consists of a uniform easterly flow ($\overline{u} = -8\ \mathrm{m\,s^{-1}}$). Since the model does not include topography, the continental outline is shown only for spatial reference. A wave train is in place after 8 days and continue to propagate westward in time. After 20 days of integration, a wave train with an approximate wavelength of 2400 km lies over the domain (Fig. 9) and continues to propagate westward in time (not shown). The amplitude of the wave train is greater within the Caribbean, which is closer to the location of the Rossby wave forcing, as compared to the eastern Pacific. In the absence of zonal and meridional variation in the basic state, the wave train continues to propagate westward and is subjected only to the damping and diffusion prescribed in the model.

The steady basic state for the simulation for the nonconvective phase of the MJO is created by averaging the 850-hPa 20-day low-pass-filtered wind, vorticity, and divergence fields for the period spanning 9–28 August 1998. This is followed up with 2 passes of a 1–2–1 spatial filter. The resulting basic-state fields, shown in Figs. 10a,b, represent a spatially and temporally smoothed version of the composite nonconvective MJO fields introduced earlier in Figs. 5a,b. As before, we note the presence of easterly flow extending across the Caribbean and the Gulf of Mexico. In the eastern Pacific, the easterlies meet southwesterlies and weak

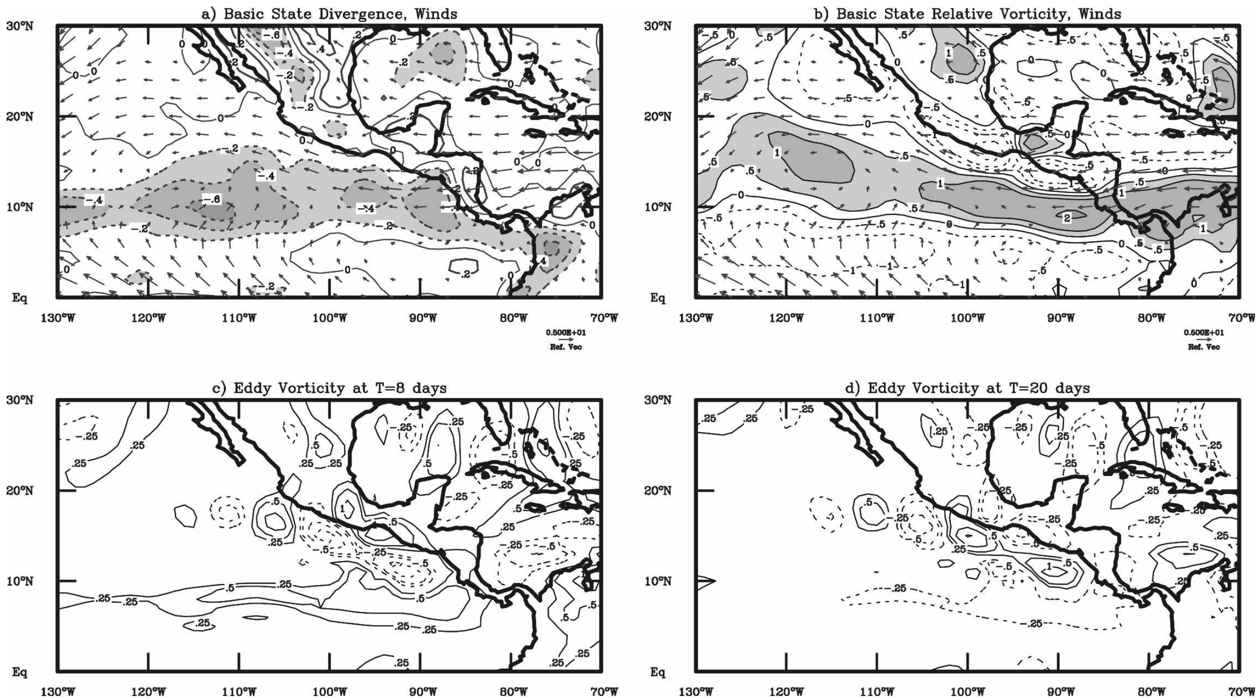

FIG. 10. (a) Divergence (negative values shaded) and (b) relative vorticity (positive values shaded) of the basic state representing the nonconvective phase of the MJO. Basic-state winds (vectors) are also shown on both panels. Shown is the eddy vorticity after (c) 8 days and (d) 20 days of integration of the barotropic model with the above basic state.

westerlies within the ITCZ, which stands out as the zonally oriented region of convergence centered at 10°N. The basic-state convergence (Fig. 10a) and relative vorticity (Fig. 10b) within the Gulf of Mexico are lower in amplitude than in the eastern Pacific.

The eddy vorticity fields after 8 days (Fig. 10c) and 20 days (Fig. 10d) show wave trains propagating into the Gulf of Mexico and the eastern Pacific. The structure of the waves differs considerably from the previous simulation with uniform easterly flow. Most notably, the wavelength is shorter in the eastern Pacific (1000 km) than in the Caribbean (1500 km). Furthermore, the largest wave amplitude occurs within the eastern Pacific. The zonal-scale contraction and amplification of the waves are consistent with the process of wave accumulation (e.g., Holland 1995; Sobel and Bretherton 1999) in response to the convergence of the basic-state flow in the eastern Pacific. The waves extending into the Gulf of Mexico have a relatively lower amplitude.

The mean EKE and barotropic conversions for this simulation are shown in Fig. 11. The pattern of the mean EKE (Fig. 11a) appears to follow that of the wave train in Fig. 10b, with centers of activity in the Atlantic, Gulf of Mexico, and north of 20°N in the eastern Pacific. Local maxima are also seen around 10°–15°N in the eastern Pacific. Figure 11b shows that the barotropic conversions are highest in the eastern Pacific. On the other hand, the eddy growth rate within the Gulf of Mexico is significantly lower.

A comparison of Figs. 11 and 7 shows that, although the pattern of the modeled and observed mean EKE differ, the barotropic conversions are broadly consistent. Over the eastern Pacific, in both the model and the observations, a zonally elongated region of eddy growth through barotropic energy exchange can be seen. Furthermore, within the Gulf of Mexico, the model simulation as well as the observations indicates limited wave growth due to barotropic conversions. It is speculated that the difference in the modeled and observed EKE near 120°W relates to the EKE contribution of the TC circulations projected on the bandpass-filtered data—an effect that is absent in the barotropic model.

The steady basic state for the simulation for the convective phase of the MJO is created by averaging the 850-hPa 20-day fields for the period spanning 29 August–17 September 1998 and 2 passes of a 1–2–1 spatial filter. The resulting basic state (Figs. 12a,b) resembles the composite fields for convective MJO phase presented earlier in Figs. 5a,b. The eddy vorticity fields after 8 days and 20 days are shown in Figs. 12c and 12d, respectively. In this simulation, the wave train extends northwestward across the Caribbean and into the Gulf of Mexico and then westward into the eastern Pacific.

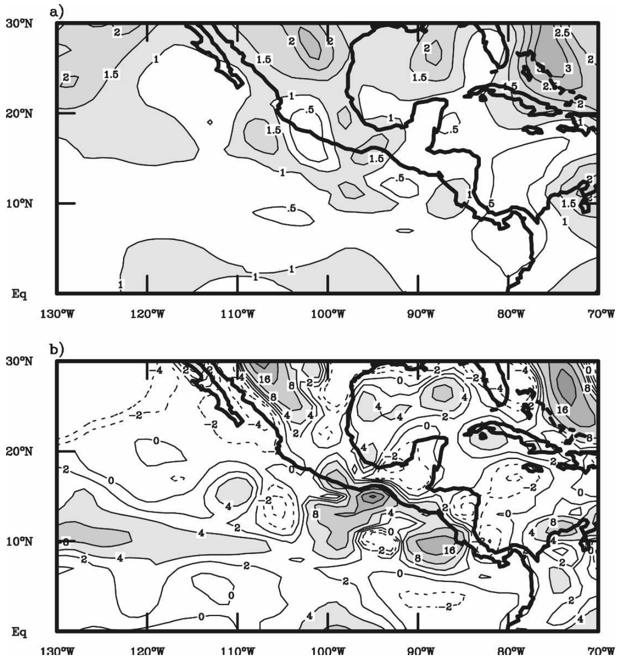

FIG. 11. (a) Mean EKE and (b) mean EKE rate of change through barotropic energy conversions for the simulation with the nonconvective MJO basic state.

This propagation is a response to the southeasterlies over the Gulf of Mexico and northwestern Caribbean in the basic state. Compared to the simulation using the nonconvective MJO basic state, the wave propagation into the eastern Pacific along the ITCZ axis is precluded by the presence of strong westerlies between 130° and 80°W. The amplitude of the waves in this case is strongest within the Gulf of Mexico.

The mean EKE and barotropic conversions for this simulation are shown in Fig. 13. The mean EKE (Fig. 13a) in this case differs significantly from the simulation using the nonconvective MJO basic state (Fig. 11a). In particular, the values within the Gulf of Mexico are 3–5 times higher in the convective MJO simulation. The mean barotropic conversions (Fig. 13b) also differ, with the most prominent departure being the strong positive values within the Gulf of Mexico. A notable feature of this simulation is that this simple model has captured, with remarkable success, the pattern of mean EKE and barotropic conversions seen in observations (cf. Figs. 8 and 13).

The barotropic conversions can be examined in detail by considering the contribution of the individual terms on the rhs of (1). The results are shown in Fig. 14. The terms $-u'v'(\partial\overline{v}/\partial x)$ (Fig. 14a) and $-u'u'(\partial\overline{u}/\partial x)$ (Fig. 14b) contribute most to positive barotropic conversions within the Gulf of Mexico. The former relates to the eddy momentum transport across the meridionally oriented jet within the eastern flank of the basic-state cyclonic gyre in the Gulf of Mexico (Fig. 12a). The latter reflects eddy growth due to the zonal wind convergence. Maloney and Hartmann (2001) and Hartmann and Maloney (2001) found that this term dominated the

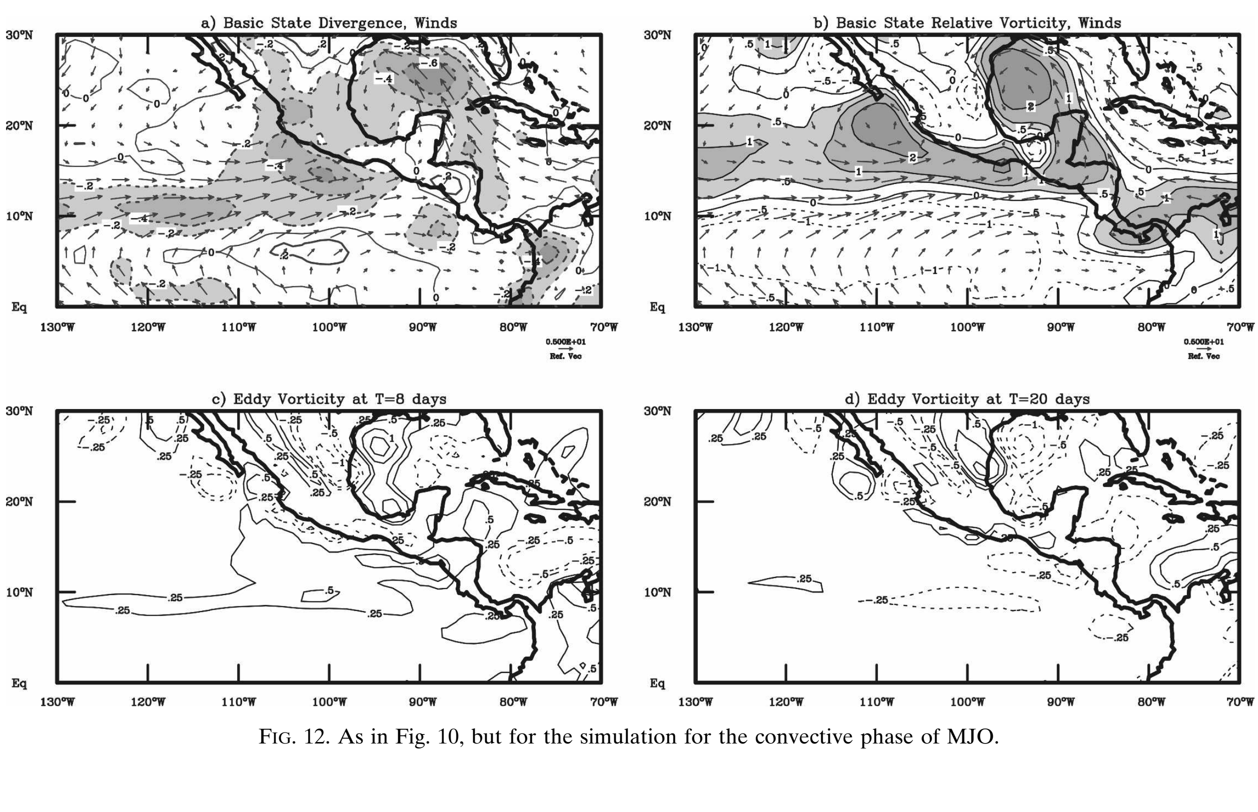

FIG. 12. As in Fig. 10, but for the simulation for the convective phase of MJO.

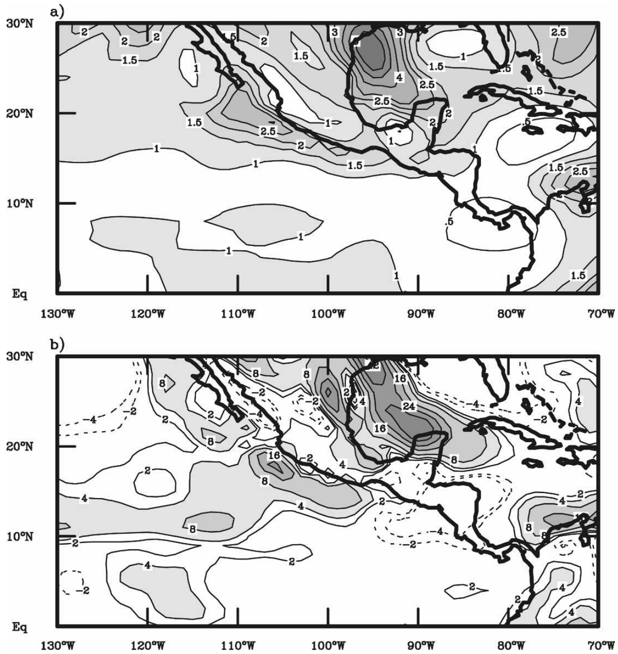

FIG. 13. As in Fig. 11, but for the simulation for the convective phase of MJO.

barotropic eddy growth over the eastern Pacific during the convective phase of the MJO. As also noted by them, this term is consistent with the mechanism of barotropic wave accumulation wherein the convergence of group velocity is associated with wave amplification (e.g., Webster and Chang 1988; Sobel and Bretherton 1999). In general, two factors contribute to the convergence of group velocity—convergence in the basic state and convergence of the flow relative group velocity through scale contraction of the waves (e.g., Kuo et al. 2001). Both factors appear to be involved here as evident from the convergence in the basic state (Fig. 12a) as well as the diminished scale of the waves within the Gulf of Mexico (Fig. 12b).

The term $-u'v'(\partial\overline{U}/\partial y)$ (Fig. 14c) produces negative barotropic conversions in both the Gulf of Mexico and the eastern Pacific. The patterns of $-u'v'(\partial\overline{v}/\partial x)$ (Fig. 14a) and $-u'v'(\partial\overline{U}/\partial y)$ (Fig. 14c) contain similar structure but opposite sign, indicating that these two terms are counteracting. However, within the Gulf of Mexico, the magnitude of the former is relatively larger and an exact cancellation of the two terms does not occur. The end result is a net positive conversion of energy from the basic state to the eddies.

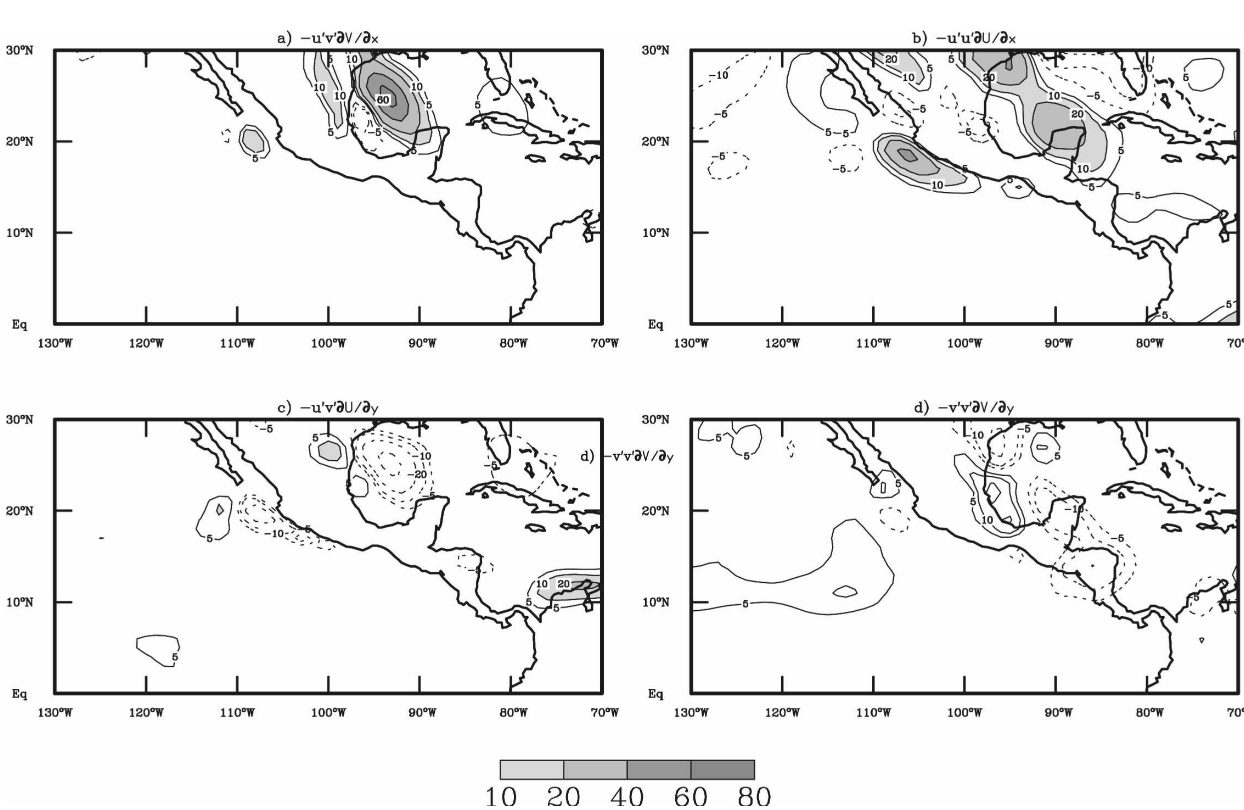

FIG. 14. The barotropic conversion terms averaged over the 480 h of simulation for the convective phase of MJO: (a) $-u'v'(\partial\overline{v}/\partial x)$, (b) $-u'u'(\partial\overline{u}/\partial x)$, (c) $-u'v'(\partial\overline{u}/\partial y)$, and (d) $-v'v'(\partial\overline{v}/\partial y)$.

The final term, $-v'v'(\partial\overline{V}/\partial y)$ (Fig. 14d), can be interpreted as the meridional counterpart of the zonal wave accumulation term $-u'u'(\partial\overline{u}/\partial x)$. This term shows positive as well as negative energy conversions within the Gulf. Here too, we note that the terms $-u'u'(\partial\overline{U}/\partial x)$ (Fig. 14b) and $-v'v'(\partial\overline{V}/\partial y)$ (Fig. 14d) tend to oppose one another. In this case, within the Gulf of Mexico, the former is much larger in magnitude and offsets the impact of the negative values of the latter.

The results in Fig. 14 show that, during the convective MJO phase, eddies in the Gulf of Mexico grow through eddy momentum transfer across the meridional jet and through zonal wave accumulation. The net barotropic conversions in Fig. 13b reflect the dominant contribution of these two terms (Figs. 14a,b).

The results of idealized simulations are consistent with the barotropic calculations based on the observed fields. The convective MJO period provides a favorable environment within the Gulf of Mexico for the growth of waves arriving from upstream. The background flow steers the waves into the Gulf during the convective phase of the MJO in contrast to the nonconvective phase where the waves continue to propagate into the eastern Pacific and amplify within the ITCZ. While these results are based on a single case study from 1998, the general principles should apply to any significant MJO event within the Gulf of Mexico.

5. Summary and discussion

During a period of 18 days spanning 31 August–17 September 1998, five TCs formed within the Gulf of Mexico and the eastern Pacific. The large-scale environment during this time showed a marked change from the conditions that existed immediately prior to this period. Convection covering a large area developed over the eastern Pacific and eventually progressed eastward and northward into the Gulf of Mexico. Concurrently, easterlies over the eastern Pacific were supplanted by westerlies and low-level cyclonic vorticity developed over a large area. This evolution of the large-scale environment is consistent with the description of the MJO for the eastern Pacific and Gulf of Mexico in past studies (e.g., Maloney and Hartmann 2000a, 2001).

On the synoptic scale, several disturbances that could be tracked back to the west coast of Africa reached the eastern Pacific and the Gulf of Mexico and amplified within the convective envelope of the MJO. It is suggested that the MJO played a leading role in the amplification of these waves in a process that culminated in the development of the aforementioned five TCs. Composite fields at the 850-hPa level show that the convective phase of the MJO is associated with low-level convergence and cyclonic relative vorticity, both conducive to tropical cyclogenesis. While Maloney and Hartmann (2000a) suggest that the convective MJO phase is also associated with a favorable pattern of vertical shear, in the present case, the vertical shear within the climatological genesis area of the eastern Pacific is much larger than in the nonconvective MJO period. Maloney and Hartmann (2000a) considered the vertical shear of only the zonal wind, citing very small meridional winds in their climatological composite. However, in this case, the contribution from the meridional winds is not negligible owing to strong cyclonic circulations associated with the MJO. Thus, in some events, the presence of strong shear during the convective phase may act to limit the number of TCs that might otherwise develop within the convective envelope of the MJO. The results also suggest that the northward shift in genesis location during the convective MJO phase is in part due to the competing influences of high vertical shear and large-scale low-level vorticity and divergence.

Barotropic energy conversions computed using ECMWF gridded analyses show enhanced eddy growth within the Gulf of Mexico and northeastern Pacific during the convective MJO phase. The regions of highest eddy growth coincide with the locations of the TC formation. Simple numerical experiments using a wave generator and background fields adapted from observations yield results that are consistent with the barotropic calculations based on gridded analyses. The numerical experiments provide further confirmation of the suggestion that the MJO environment is conducive for the amplification of easterly waves arriving from upstream. They also show that the propagation of these waves is influenced by the MJO-related environmental flow. During the nonconvective phase, the waves primarily tended to propagate westward into the eastern Pacific, but during the convective phase they propagated northward into the Gulf of Mexico.

While the barotropic framework provides a simple avenue for understanding the role of the MJO, the importance of convective feedbacks in the growth of the waves cannot be ignored. However, as noted in previous studies (e.g., Molinari et al. 1997; Maloney and Hartmann 2000), large-scale barotropic dynamics can play a key role in the amplification of weak precursor disturbances at least until they reach sufficient amplitude to sustain the feedback processes that can lead to the cyclogenesis.

The results of this study raise several issues that need to be further examined. These include the following. (i) How often do strong MJO events such as the one highlighted by the present case occur within the Gulf of Mexico? (ii) Since the easterly waves are steered into the Gulf of Mexico by the environmental flow associated with the convective MJO phase, does this reduce the wave activity within the eastern Pacific? (iii) What is the relative importance of the MJO's role as compared to other processes such as the influence of the topography (e.g., Zehnder 1991; Zehnder and Gall 1991), ITCZ breakdown (e.g., Ferreira and Schubert 1997), and upper-level potential vorticity influences (e.g., Bosart and Bartlo 1991)? It is expected that a resolution of these issues will lead to a better understanding of the process of tropical cyclogenesis associated with the MJO in the Gulf of Mexico and eastern Pacific.

Acknowledgments. This work was supported by National Science Foundation Grant ATM 0201752 and Office of Naval Research Grant N00014-02-10821. We are also grateful to four anonymous reviewers for their valuable and constructive comments.

REFERENCES

Avila, L. A., and J. L. Guiney, 2000: Eastern North Pacific hurricane season of 1998. *Mon. Wea. Rev.,* **128,** 2990–3000.

Bosart, L. F., and J. A. Bartlo, 1991: Tropical storm formation in a baroclinic environment. *Mon. Wea. Rev.,* **119,** 1979–2013.

Carlson, T. N., 1969: Some remarks on African disturbances and their progress over the tropical Atlantic. *Mon. Wea. Rev.,* **97,** 716–726.

Duchon, C. E., 1979: Lanczos filtering in one and two dimensions. *J. Appl. Meteor.,* **18,** 1016–1022.

Emanuel, K., 1986: An air–sea interaction theory for tropical cyclones. Part I: Steady-state maintenance. *J. Atmos. Sci.,* **45,** 585–604.

Ferreira, R. N., and W. H. Schubert, 1997: Barotropic aspects of ITCZ breakdown. *J. Atmos. Sci.,* **54,** 261–285.

Gray, W. M., 1968: Global view of the origin of tropical disturbances and storms. *Mon. Wea. Rev.,* **96,** 669–700.

Hall, J. D., A. J. Matthews, and D. J. Karoly, 2001: The modulation of tropical cyclone activity in the Australian region by the Madden–Julian oscillation. *Mon. Wea. Rev.,* **129,** 2970–2982.

Hartmann, D. L., and E. D. Maloney, 2001: The Madden–Julian oscillation, barotropic dynamics, and North Pacific tropical cyclone formation. Part II: Stochastic barotropic modeling. *J. Atmos. Sci.,* **58,** 2559–2570.

Hodges, K. I., D. W. Chappell, G. J. Robinson, and G.-Y. Yang, 2000: An improved algorithm for generating global window brightness temperatures from multiple satellite infrared imagery. *J. Atmos. Oceanic Technol.,* **17,** 1296–1312.

Holland, G. J., 1995: Scale interaction in the western Pacific monsoon. *Meteor. Atmos. Phys.,* **56,** 57–79.

Kuo, H.-C., J.-H. Chen, R. T. Williams, and C.-P. Chang, 2001: Rossby waves in zonally opposing mean flow: Behavior in Northwest Pacific summer monsoon. *J. Atmos. Sci.,* **58,** 1035–1050.

Liebmann, B., H. H. Hendon, and J. D. Glick, 1994: The relationship between tropical cyclones of the western Pacific and Indian Oceans and the Madden–Julian oscillation. *J. Meteor. Soc. Japan,* **72,** 401–412.

Madden, R. A., and P. R. Julian, 1971: Detection of a 40–50 day oscillation in the zonal wind in the tropical Pacific. *J. Atmos. Sci.,* **28,** 702–708.

Maloney, E. D., and D. L. Hartmann, 2000a: Modulation of eastern North Pacific hurricanes by the Madden–Julian oscillation. *J. Climate,* **13,** 1451–1460.

——, and ——, 2000b: Modulation of hurricane activity in the Gulf of Mexico by the Madden–Julian oscillation. *Science,* **287,** 2002–2004.

——, and ——, 2001: The Madden–Julian oscillation, barotropic dynamics, and North Pacific tropical cyclone formation. Part I: Observations. *J. Atmos. Sci.,* **58,** 2545–2558.

McBride, J. L., and R. Zehr, 1981: Observational analysis of tropical cyclone formation. Part II: Comparison of non-developing versus developing systems. *J. Atmos. Sci.,* **38,** 1132–1151.

Molinari, J., and D. Vollaro, 1990: External influences on hurricane intensity. Part II: Vertical structure and response of the hurricane vortex. *J. Atmos. Sci.,* **47,** 1902–1918.

——, and ——, 2000: Planetary- and synoptic-scale influences on eastern Pacific tropical cyclogenesis. *Mon. Wea. Rev.,* **128,** 3296–3307.

——, ——, and F. Robasky, 1992: Use of ECMWF operational analyses for studies of the tropical cyclone environment. *Meteor. Atmos. Phys.,* **47,** 127–144.

——, D. Knight, M. Dickinson, D. Vollaro, and S. Skubis, 1997: Potential vorticity, easterly waves, and eastern Pacific tropical cyclogenesis. *Mon. Wea. Rev.,* **125,** 2699–2708.

Nakazawa, T., 1986: Intraseasonal variation of OLR in the tropics during the FGGE year. *J. Meteor. Soc. Japan,* **64,** 17–34.

Palmen, E. H., 1948: On the formation and structure of tropical cyclones. *Geophysica,* **3,** 26–38.

Pasch, R. J., L. A. Avila, and J. L. Guiney, 2001: Atlantic hurricane season of 1998. *Mon. Wea. Rev.,* **129,** 3085–3123.

Sobel, A. H., and C. S. Bretherton, 1999: Development of synoptic-scale disturbances over the summertime tropical Northwest Pacific. *J. Atmos. Sci.,* **56,** 3106–3127.

——, and E. D. Maloney, 2000: Effect of ENSO and the MJO on western North Pacific tropical cyclones. *Geophys. Res. Lett.,* **27,** 1739–1742.

Sweet, R. A., 1977: A cyclic reduction algorithm for solving block tridiagonal systems of arbitrary dimensions. *SIAM J. Numer. Anal.,* **14,** 706–720.

Webster, P. J., and H.-R. Chang, 1988: Equatorial energy accumulation and emanation regions: Impacts of a zonally varying basic state. *J. Atmos. Sci.,* **45,** 803–829.

Wheeler, M., and G. N. Kiladis, 1999: Convectively coupled equatorial waves: Analysis of clouds and temperature in the wavenumber–frequency domain. *J. Atmos. Sci.,* **56,** 374–399.

Wiin-Nielsen, A., 1961: On short- and long-term variations in quasi-barotropic flow. *Mon. Wea. Rev.,* **89,** 461–476.

Zehnder, J. A., 1991: The interaction of planetary-scale tropical easterly waves with topography: A mechanism for the initiation of tropical cyclones. *J. Atmos. Sci.,* **48,** 1217–1230.

——, and R. L. Gall, 1991: Alternative mechanisms of tropical cyclone formation in the Eastern North Pacific. *Atmósfera,* **4,** 37–51.

Zehr, R. M., 1992: Tropical cyclogenesis in the western North Pacific. NOAA Tech. Rep. NESDIS 61, 181 pp.